Comparison of Calibrated Two-equation Turbulence Models with LES and Experimental Results for Flow Around a High-rise Building

o Mohammadreza Shirzadi, Postdoctoral Research Fellow, Wind and Fluid Engineering Research Center, Niigata Institute of Technology, Shirzadi.mr@gmail.com
Yoshihide Tominaga, Professor, Wind and Fluid Engineering Research Center, Niigata Institute of Technology, tominaga@abe.niit.ac.jp

In this study, a calibration procedure for RANS turbulence model modification is proposed and applied to flow around a high-rise building as a case study. Wind tunnel measurements for the velocity and turbulent kinetic energy over 853 measurement points around the building were utilized to define validation metrics, which then used as the objective function in the optimization solver which was developed for calibration. Results of the calibrated RANS model were compared with experimental measurement data as well as LES results. Different flow parameters were compared in order to investigate the limitation and physical meaning of the calibrate CFD model.

1. Introduction

Computational fluid dynamics (CFD) is utilized in many different urban-related studies to obtain a high-resolution distribution of flow parameters. Many successful applications of CFD were reported for applications of the pedestrian-level wind comfort [1], the pollution dispersion [2], the building energy consumption [3], the wind energy [4], and the urban heat island [5].

In the field of urban environment study, two different approaches are widely used in CFD, i.e., the Reynolds Averaged Navier-Stokes equations (RANS) model and large eddy simulations (LES). LES resolves the Navier-Stokes equations in time and space over the sub-grid scale and provides higher accurate results in comparison to RANS, but it requires noticeable computational resources. Furthermore, there are a many challenging issues for grid sensitivity and transient boundary condition implementation for LES, which make it infeasible for urban airflow simulations [6].

RANS models are widely used in many engineering applications thanks to their lower computational cost and implementation complexity. Despite the popularity of RANS, their accuracy in prediction of flow parameters in weak wind regions behind buildings and street canyons in dense urban areas is low. They generally underestimate momentum diffusion in these regions which is accompanied by underestimation of turbulent kinetic energy (TKE) [7]. One reason of such inaccuracy is due to the RANS turbulence models parameters which are historically developed for fundamental flows in fluid dynamics, including simple shear flow, homogeneous isotropic decaying flow, and fully developed channel flow [8]. Nevertheless, these flows have few similarity with the airflow in the atmospheric boundary layer (ABL) around buildings in urban areas [9].

Hence, in this study a procedure for improving the accuracy of RANS for airflow CFD simulations is presented which is based on the closure coefficients calibration using wind tunnel measurements. The method was applied to a case study of flow around a high-rise building model. Details of the flow quantities were compared with experimental measurements as well as LES results.

2. Calibration method of RANS closure coefficients

In Figure 1, the procedure for RANS parameter calibration is shown. Input parameters for RANS calibration are the closure coefficients of RANS turbulence models, which should be determined in the first step. In the next step, a sensitivity study will be carried out using Monte Carlo sampling technique. By coupling the Monte Carlo sampling technique and RANS CFD simulations, closure coefficients will be randomly varied in accordance with their given probability distribution functions (PDFs). The RANS CFD simulations will be repeatedly run to characterize the statistical parameters of the validation metrics, including their mean and standard deviation values. By integrating the Monte Carlo sampling into an optimizer, not only can the best mean value of validation metrics is calculated, but it is also possible to minimize the standard deviation of the validation metrics so as to reduce the effects of uncertainty of the closure coefficients on the validation metrics. Nonlinear Programing with Non-Monotone and Distributed Line Search (NLPQLP) optimization method [10], is used for the optimization purpose.

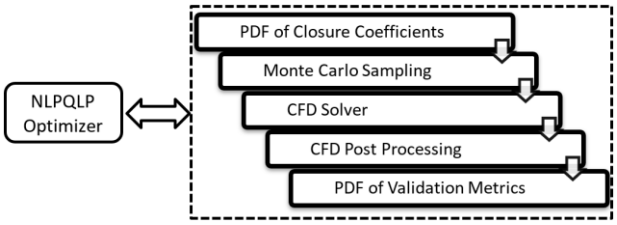

Figure 1 Procedure for RANS parameter calibration.

The stochastic optimization is defined to find a set of closure coefficients (X) that:

Minimize: $f(\mu_y(X), \sigma_y(X))$

Subject to: $X_L \leq X \leq X_U$ (1)

where X_L and X_U are the lower and upper limits for closure coefficients X. A weighted sum approach was used to define the objective function, which includes a term for mean value variation relative to the target and a term to minimize the standard deviation of validation metrics [11]:

$$F = \sum_{i=1}^{l} \left[\frac{w_{1_i}}{s_{1_i}} \left(\mu_{y_i} - M_i \right)^2 + \frac{w_{2_i}}{s_{2_i}} \sigma_{y_i}^2 \right] \quad (2)$$

where w_{1_i} and w_{2_i} are the weighting factors, and s_{1_i} and s_{2_i}

are the scale factors related to each term. M_i stands for the target of validation metric i and l is the total number of validation metrics. The statistical variability of validation metrics (i.e. μ_{y_i} and σ_{y_i}), which are required by the stochastic optimization formulation, can be estimated using Monte Carlo simulation (MCS) technique. More details about the stochastic optimization can be found in [12].

3. CFD modeling

3.1. RANS turbulence model description

The two RANS turbulence models are considered in this study, i.e., the standard $k-\varepsilon$ model (Std k-ε) [13] and the standard $k-\varepsilon$ model with LK modification (LK $k-\varepsilon$) [14] model. The Reynolds stress is calculated based on the gradient diffusion hypothesis:

$$-\rho\overline{u_i u_j} = \mu_t\left(\frac{\partial U_i}{\partial x_j}+\frac{\partial U_j}{\partial x_i}\right)-\frac{2}{3}\delta_{ij}\rho k \quad (3)$$

where U_i and u_i are respectively component of the mean and instantaneous velocity in streamwise, lateral, and vertical directions, ρ is air density, and μ_t is the eddy viscosity (turbulent viscosity), which can be defined as below:

$$\mu_t = C_\mu \rho \frac{k^2}{\varepsilon} \quad (4)$$

Values of the turbulent kinetic energy (k) and its dissipation rate (ε) come directly from their differential transport equations:

$$\frac{\partial \rho U_j k}{\partial x_j} = \frac{\partial}{x_j}\left[\left(\mu+\frac{\mu_t}{\sigma_k}\right)\frac{\partial k}{x_j}\right]+P_k-\rho\varepsilon \quad (5)$$

$$\frac{\partial \rho U_j \varepsilon}{\partial x_j} = \frac{\partial}{x_j}\left[\left(\mu+\frac{\mu_t}{\sigma_\varepsilon}\right)\frac{\partial \varepsilon}{x_j}\right]+\frac{\varepsilon}{k}(C_{\varepsilon 1}P_k-C_{\varepsilon 2}\rho\varepsilon) \quad (6)$$

where μ is molecular viscosity and P_k is the production of turbulence due to shear. In the std $k-\varepsilon$ model, P_k is defined as:

$$P_k = \mu_t S^2 \quad (7)$$

where $S=\sqrt{2S_{ij}S_{ij}}$ is the magnitude of strain rate. In the LK $k-\varepsilon$ model, P_k is defined as follows:

$$P_k = \mu_t S\Omega \quad (8)$$

where $\Omega=\sqrt{2\Omega_{ij}\Omega_{ij}}$ is the magnitude of vorticity rate. The vorticity tensor Ω_{ij} is calculated as below:

$$\Omega_{ij} = \frac{1}{2}\left(\frac{\partial U_i}{\partial x_j}-\frac{\partial U_j}{\partial x_i}\right) \quad (9)$$

Values of the closure coefficients for the Std and LK $k-\varepsilon$ models, according to [15], are predefined as the default values for most of the popular CFD tools such as ANSYS CFX, ANSYS FLUENT, STAR-CCM+, and OPenFoam, as below:

$$C_\mu = 0.09, C_{\varepsilon 1} = 1.44, C_{\varepsilon 2} = 1.92, \sigma_k = 1, \sigma_\varepsilon = 1.3 \quad (10)$$

3.2. Numerical setup

Air flow around a high-rise building model with 1:1:2 shape was predicted by steady RANS and LES models. ANSYS FLUENT was utilized for all CFD calculations. For RANS, the SIMPLE algorithm utilized for the pressure-velocity coupling while the 2nd order upwind scheme was used for advection term discretization. For LES, the PISO solver was used for the pressure-velocity coupling and the bounded central differencing approach was used for the momentum equation spatial discretization. The transient formulation was based on the second order implicit scheme. The standard Smagorinsky model was used with the Smagorinsky constant 0.12. The statistics were calculated for 34 seconds in real time which corresponds to 1655 non-dimensional time unit.

The computational domain is shown in Figure 2, which is a rectangular domain discretized using hexahedral structured cell elements with a cell number of about 928,136. The same computational domain and grid are used for both RANS and LES. The details of grid discretization are reported in [16].

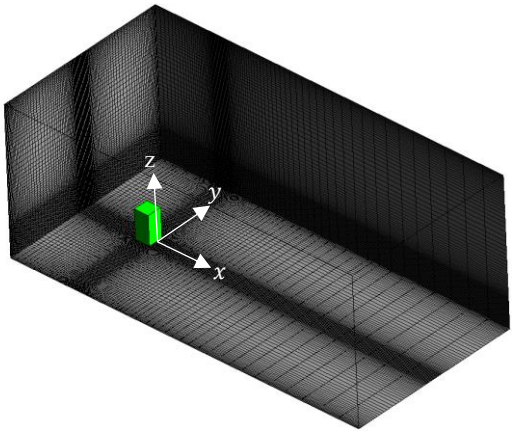

Figure 2 Computational domain for high-rise building.

For the Inlet boundary condition for LES, the vortex method with 1000 vortices, which is implemented in Fluent, was used to generate instantaneous fluctuated velocities at the inlet boundary. The vertical profiles of the streamwise velocity $\left(\frac{U}{U_H}\right)$ and TKE $\left(\frac{k}{U_H^2}\right)$ are shown in Figure 3. The obtained inflow profiles by LES was used for RANS in order to minimize the effect of the inflow boundary condition on the prediction results for comparison.

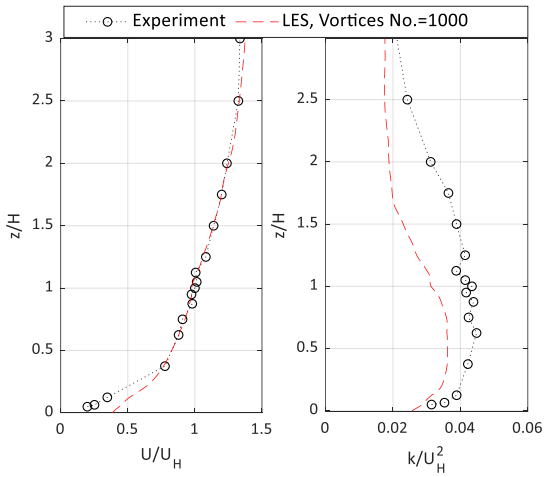

Figure 3 Vertical profiles of the mean streamwise velocity and TKE used as inlet boundary condition.

4. Wind tunnel measurements

Experimental data for $\left(\frac{U}{U_H}\right)$ and $\left(\frac{k}{U_H^2}\right)$ was obtained from extensive wind tunnel measurements conducted in the open-circuit wind tunnel at Tokyo Polytechnic University, Japan [16]. The three

components of velocity were measured by the sprit fiber probe and CTA module [17]. The experimentally obtained mean-velocity components and TKE over 853 points, which are located over a vertical plane at $\frac{y}{H} = 0$ and two horizontal planes at $\frac{z}{H} = 0.0625$ and $\frac{z}{H} = 0.5$, as shown in Figure 4, were used for the calibration.

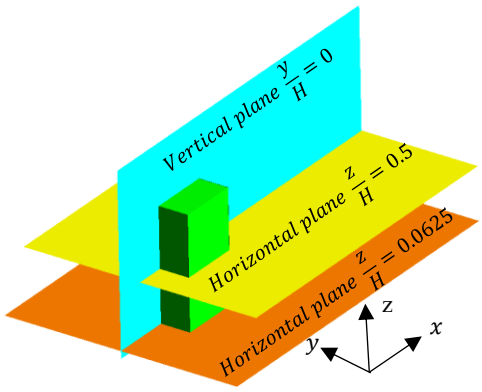

Figure 4 Measurement location in the wind tunnel experiment used for RANS calibration.

5. Results and discussion

5.1. Calibration results

In Table 1, the values of the default and calibrated coefficients are listed. The different values are obtained for the calibrated Std $k-\varepsilon$ and LK $k-\varepsilon$ models, but the direction of calibrated values is the same. For instance, the calibrated values for C_μ are 0.077 and 0.056 for the calibrated Std and LK $k-\varepsilon$ models, which are lower than the default values of 0.09.

Table 1 Values of closure coefficients for default and calibrated models

	C_μ	$C_{\varepsilon 1}$	$C_{\varepsilon 2}$	σ_k	σ_ε
Std $k-\varepsilon$ / LK $k-\varepsilon$	0.09	1.44	1.92	1.0	1.3
Calibrated Std $k-\varepsilon$	0.077	1.47	2.65	0.76	0.51
Calibrated LK $k-\varepsilon$	0.056	1.44	3.11	0.64	0.42

5.2. Distribution of the mean velocity and TKE

In Figure 5, the streamlines and the distribution of $\frac{U}{U_H}$ is shown over a vertical plane at $\frac{y}{H} = 0$. The LES results show very good agreement in comparison with the experiment where the size of the wake region behind the building is predicted accurately. Distributions of $\frac{U}{U_H}$ obtained by the Std and LK $k-\varepsilon$ models show clearly the well-known tendency of steady RANS models in under-prediction of momentum diffusion behind the building [7]. In contrast, the calibrated Std and LK $k-\varepsilon$ models show significant improvement in this region, where the wake length behind the building is noticeably shorter than the one predicted by the Std and LK $k-\varepsilon$ models.

The distributions of $\frac{U}{U_H}$ over a horizontal plane near the ground at $\frac{z}{H} = \frac{1}{16}$ is shown in Figure 6. For the Std and LK $k-\varepsilon$ models with the default closure coefficients, a very long recirculating flow is predicted which is resulted due to the momentum diffusion underprediction in this area. The calibrated models, in contrast, show very close agreement with LES and experiment results where the shorter recirculating flow is predicted in comparison with the default models.

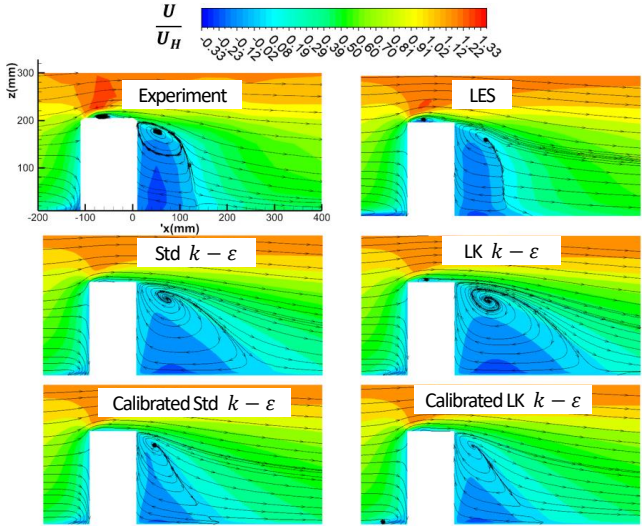

Figure 5 Distribution of the streamwise velocity over the vertical plane at $\frac{y}{H} = 0$.

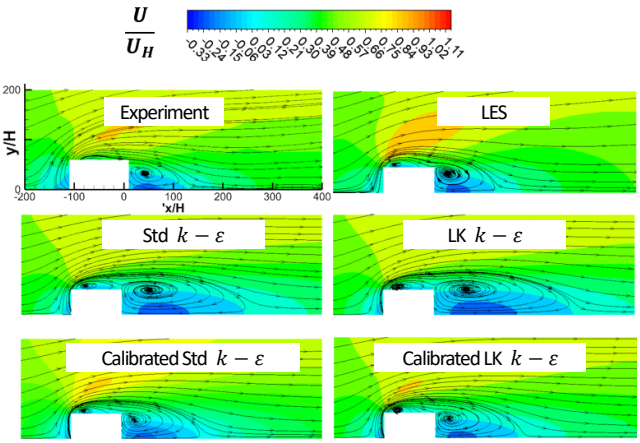

Figure 6 Distribution of the streamwise velocity over the horizontal plane at $\frac{z}{H} = \frac{1}{16}$.

In Figure 7, the profiles of $\frac{U}{U_H}$ are plotted for the different turbulence models and compared with experimental results. Over the vertical plane at $\frac{y}{H} = 0$ and horizontal plane at $\frac{z}{H} = 0.5$, very close agreements between all CFD models and experimental results are obtained in front of the building and over the roof and sidewalls ($\frac{x}{H} = -0.75$ and $\frac{x}{H} = -0.25$). The velocity prediction inside the wake region clearly reveals the over-prediction of the reverse flow by the Std and LK $k-\varepsilon$ models, while noticeable prediction improvement by the calibrated models is clearly observed at $\frac{x}{H} = 0.75$ and $\frac{x}{H} = 1.25$.

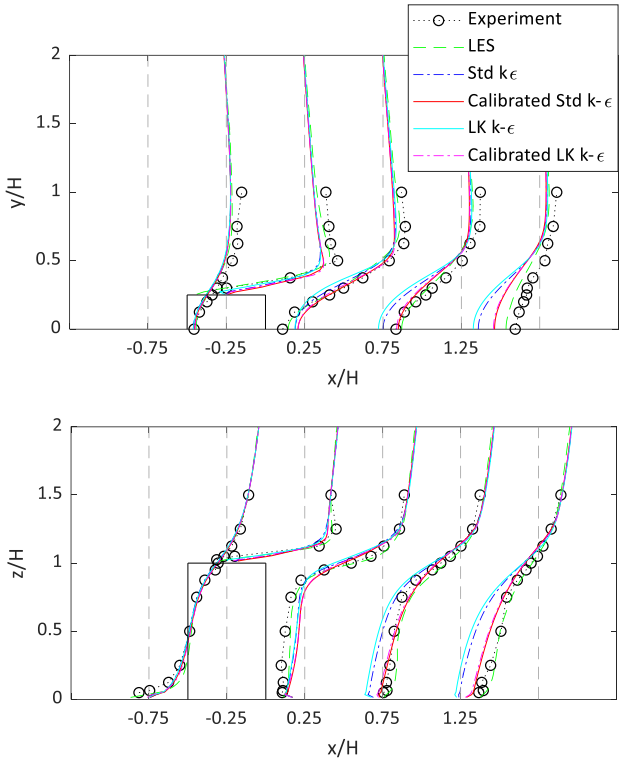

Figure 7 Profiles of the streamwise velocity over (a) horizontal plane at $\frac{z}{H} = 0.5$ and (b) vertical plan at $\frac{y}{H} = 0$.

The distribution of $\frac{k}{U_H^2}$ at $\frac{y}{H} = 0$ is depicted in Figure 8. The results of LES and experiment show high level of the TKE above the building roof and in the wake behind the building. The Std $k - \varepsilon$ model predicted the large value of TKE near the stagnation point in front of the building. It is due to the over-estimation of the production term in this model caused by the diagonal elements of the strain tensor which are very high around stagnation region [18]. Modification of the production term implemented in the LK $k - \varepsilon$ model, reduces the TKE around the stagnation point. Nevertheless, both models noticeably underestimate TKE in the wake region. As can be seen in the figure, the calibrated models predict TKE more accurately in the wake region. Nonetheless, TKE is overpredicted above the roof by two calibrated models.

The TKE distribution over the horizontal plane at $\frac{z}{H} = \frac{1}{16}$, is shown in Figure 9. While the Std $k - \varepsilon$ predicts larger value of TKE in front of the building, the LK $k - \varepsilon$ model shows better accuracy when compared with LES and experiment. However, at the downwind of the sidewalls, the high TKE region is observed in the experiment and LES, but the both models with default closure coefficients failed to reproduce it accurately. By utilizing the calibrated coefficients, TKE prediction accuracy is improved not only near the sidewall but also in the reverse flow region behind the building, as shown in the figure.

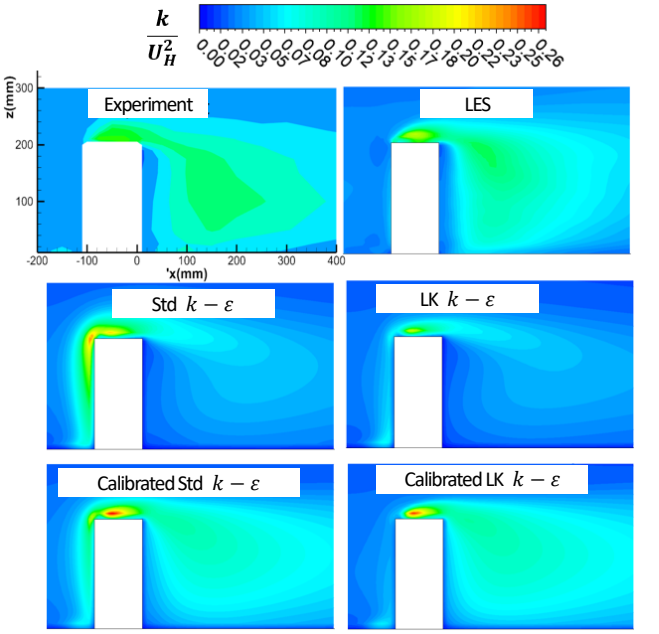

Figure 8 Distribution of the TKE over the vertical plane at $\frac{y}{H} = 0$.

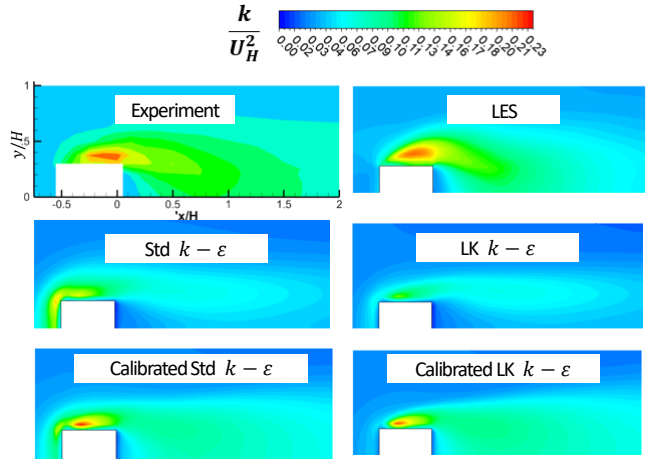

Figure 9 Distribution of TKE over the horizontal plane at $\frac{z}{H} = \frac{1}{16}$.

The profiles of $\frac{k}{U_H^2}$ over the same vetical and horizontal planes are shown in Figure 10. In front of the builidng at $\frac{x}{H} = -0.75$, all CFD models calculate TKE accuratley with slighlty over-prediction between $0.5 \leq \frac{z}{H} \leq 1$ by the Std $k - \varepsilon$ and calibrated Std $k - \varepsilon$ models. Around the sidewall at $\frac{x}{H} = -0.25$ and behind the building, the performance of calibrated models shows definite superiority in comparison to the models with the default coefficients. However, over the roof area $\left(\frac{x}{H} = -0.25\right)$ around $1 \leq \frac{z}{H} \leq 1.2$, the calibrated models show slight over-prediction in comparison to the

experimental data.

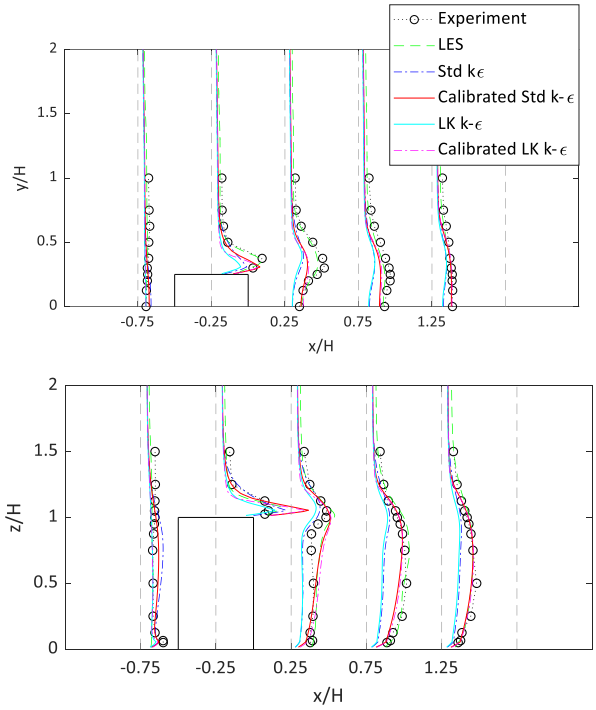

Figure 10 Profiles of the TKE over (a) horizontal plane at $\frac{z}{H} = 0.5$ *and (b) vertical plan at* $\frac{y}{H} = 0$.

5.3. Validation metrics for the mean velocity components and TKE

A quantitative comparison by using the validation metrics is performed for three mean velocity components and TKE over 853 measurement points, as shown in Table 2. The comparison of the validation metrics obtained by the default and calibrated models shows the accuracy improvement of the calibrated models. For instance, $FAC2_U$ and $FAC2_k$ for the default Std $k-\varepsilon$ model are 0.76 and 0.68, respectively, while they are 0.88 and 0.83 for the calibrated Std $k-\varepsilon$ model. These values are $FAC2_U = 0.93$ and $FAC2_k = 0.97$ for LES.

Table 2 Validation metrics for $\frac{U}{U_H}$ *and* $\frac{k}{U_H^2}$

	LES	*Std* $k-\varepsilon$	*LK* $k-\varepsilon$	*Modified Std* $k-\varepsilon$	*Modified LK* $k-\varepsilon$
$FAC2_U$	*0.93*	*0.76*	*0.73*	*0.88*	*0.87*
$FAC2_V$	*0.94*	*0.82*	*0.81*	*0.85*	*0.84*
$FAC2_W$	*0.8*	*0.76*	*0.76*	*0.76*	*0.76*
$FAC2_k$	*0.97*	*0.68*	*0.65*	*0.83*	*0.85*
q_U	*0.86*	*0.61*	*0.59*	*0.71*	*0.71*
q_V	*0.92*	*0.73*	*0.73*	*0.79*	*0.79*
q_w	*0.78*	*0.74*	*0.73*	*0.75*	*0.74*
q_k	*0.84*	*0.18*	*0.09*	*0.38*	*0.39*
FB_k	*0.12*	*0.34*	*0.55*	*0.19*	*0.26*
$NMSE_k$	*0.05*	*0.53*	*0.57*	*0.24*	*0.2*

The very close results, in terms of validation metrics for the mean velocity components, are obtained by the calibrated Std $k-\varepsilon$ and calibrated LK $k-\varepsilon$ models. $FAC2_U$, $FAC2_V$, and $FAC2_W$ are respectively 0.88, 0.85, and 0.76 for the calibrated Std $k-\varepsilon$ model while they are respectively 0.87, 0.84, and 0.76 for the calibrated LK $k-\varepsilon$ model.

As shown in Figure 8 and Figure 9, the TKE prediction by the calibrated LK $k-\varepsilon$ model is noticeably more accurate than the calibrated Std $k-\varepsilon$ near the stagnation point. Nevertheless, very close values are obtained by the calibrated models for $FAC2_k$ and q_k, which are respectively 0.83 and 0.38 for the calibrated Std $k-\varepsilon$ model and 0.85 and 0.39 for the calibrated LK $k-\varepsilon$ model.

Variations of FB_k and $NMSE_k$ are more different for the calibrated models. While for the Std $k-\varepsilon$ and LK $k-\varepsilon$ models FB_k and $NMSE_k$ are respectively 0.34, 0.55 and 0.55, 0.57, they decrease to 0.19, 0.24 and 0.26, 0.20 for the calibrated Std $k-\varepsilon$ and calibrated LK $k-\varepsilon$ models, respectively. For LES $FB_k = 0.12$ and $NMSE_k = 0.05$.

6. Conclusion

A methodology for calibration of RANS model's parameters was introduced. The method was applied to the Std and LK $k-\varepsilon$ models for predicting flow parameters around a high-rise building. The results were compared with wind tunnel measurement data and LES results. Model improvement achieved by the calibrated models were discussed for the mean-velocity components and TKE distributions around the building.

References

(1) P.A. Mirzaei, F. Haghighat, "A novel approach to enhance outdoor air quality: Pedestrian ventilation system", Build. Environ. 45 (2010) 1582–1593.

(2) F. Haghighat, P.A. Mirzaei, "Impact of non-uniform urban surface temperature on pollution dispersion in urban areas", Build. Simul., Springer, (2011) 227–244.

(3) R. Evins, J. Allegrini, P. Moonen, "Emulating site-specific wind flow information for use in building energy simulations", Build. Simul. Optim. (2014), London, UK.

(4) P.A. Mirzaei, M. Rad, "Toward design and fabrication of wind-driven vehicles: Procedure to optimize the threshold of driving forces", Appl. Math. Model. 37 (2013) 50–61.

(5) Y. Kawamoto, "Effect of Urbanization on the Urban Heat Island in Fukuoka-Kitakyushu Metropolitan Area, Japan", Procedia Eng. 169 (2016) 224–231.

(6) B. Blocken, LES over RANS in building simulation for outdoor and indoor applications: A foregone conclusion?, Build. Simul. 11 (2018) 821–870.

(7) Y. Tominaga, "Flow around a high-rise building using steady and unsteady RANS CFD: Effect of large-scale fluctuations on the velocity statistics", J. Wind Eng. Ind. Aerodyn. 142 (2015) 93–103.

(8) S.B. Pope, "Turbulent flows", (2001).

(9) M. Shirzadi, P.A. Mirzaei, M. Naghashzadegan, "Improvement of k-epsilon turbulence model for CFD simulation of atmospheric boundary layer around a high-rise building using stochastic optimization and Monte Carlo Sampling technique", J. Wind Eng. Ind. Aerodyn. 171 (2017) 366-379.

(10) K. Schittkowski, "NLPQLP: A Fortran implementation of a sequential quadratic programming algorithm with distributed and non-monotone line search-user's guide", (2006).

(11) P.N. Koch, R.-J. Yang, L. Gu, "Design for six sigma through robust optimization, Struct". Multidiscip. Optim. 26 (2004)

235–248.

(12) M. Shirzadi, P.A. Mirzaei, M. Naghashzadegan, Y. Tominaga, "Modelling enhancement of cross-ventilation in sheltered buildings using stochastic optimization", Int. J. Heat Mass Transf. 118 (2018) 578-772.

(13) B.E. Launder, D.B. Spalding, "The numerical computation of turbulent flows", Comput. Methods Appl. Mech. Eng. 3 (1974) 269–289.

(14) M. Kato, B.E. Launder, "The modelling of turbulent flow around stationary and vibrating square cylinders", Turbul. Shear Flow. 1 (1993) .

(15) B.E. Launder, B.I. Sharma, "Application of the energy-dissipation model of turbulence to the calculation of flow near a spinning disc", Lett. Heat Mass Transf. 1 (1974) 131–137.

(16) T. Okaze, H. Kikumoto, H. Ono, M. Imano, T. Hasama, T. Kishida, K. Nakao, N. Ikegaya, Y. Tabata, Y. Tominaga, "Large-eddy simulations of flow around a high-rise building-validation and sensitivity analysis on turbulent statistics", in: Proc. 7th Eur. African Conf. Wind Eng. Liege, Belgium, (2017) 3–6.

(17) H. Tanaka, R. Yoshie, C.-H. Hu, "Uncertainty in measurements of velocity and concentration around a building", in: 4th Int. Symp. Comput. Wind Eng., (2006) 549–552.

(18) S. Murakami, R. Ooka, S. Kato, S. Iizuka, A. Mochida, "Numerical prediction of flow around a building with various turbulence models: Comparison of k-ε EVM, ASM, DSM, and LES wind tunnel tests", American Society of Heating, Refrigerating and Air-Conditioning Engineers , (1996).